RESEARCH

A Fluorescent and Colorimetric Chemosensor Detecting Pd²⁺ Based on Chalcone Structure with Triphenylamine

Sungjin Moon[1] · **Cheal Kim**[1]

Abstract

A fluorometric and colorimetric chemosensor **DiPP** ((*E*)-3-(4-(diphenylamino)phenyl)-1-(pyridin-2-yl)prop-2-en-1-one) based on chalcone structure with a triphenylamine group was synthesized. Sensor **DiPP** detected Pd²⁺ with fluorescence turn-off and via colorimetry variation of yellow to purple. The binding ratio of **DiPP** to Pd²⁺ turned out to be 1 : 1. Detection limits for Pd²⁺ by **DiPP** were analyzed to be 0.67 μM and 0.80 μM through the fluorescent and colorimetric methods. Additionally, the fluorescent and colorimetric test strips were applied for probing Pd²⁺ and displayed that **DiPP** could obviously discriminate Pd²⁺ from other metals. The binding feature of **DiPP** to Pd²⁺ was presented by ESI-mass, Job plot, NMR titration, ESI-mass, and DFT calculations.

Keywords Pd²⁺ · Fluorometric chemosensor · Colorimetric chemosensor · DFT · Test strip

Introduction

Palladium is a widely used transition metal in various fields such as pharmaceutical synthesis, electrical and electronic industries, medical devices, automobiles, and catalysts [1–3]. A large number of palladium ions are released as they are used for various purposes, and the released palladium ions have a harmful effect on the environment and the human body [4–7]. Therefore, it is required to develop methods capable of easily and quickly detecting palladium ions [8, 9].

To detect Pd²⁺, there are various analytical methods like inductively coupled plasma mass spectrometry, X-ray fluorescence (XRF), solid-phase micro-extraction coupled high-performance liquid chromatography, and atomic absorption spectrometry [10–12]. However, these analytical methods require expensive equipment, trained professionals, and prolonged sample preparation time [13–17]. Due to these shortcomings, chemosensors are attracting attention as an alternative analytical method [18–21]. Chemosensors have advantages such as high sensitivity, specificity, fast response, and technical simplicity [22–28].

Pyridine can endow cations with a binding site through a lone pair electron of nitrogen atom [29–31]. Also, fluorophores including pyridine moiety are known to exhibit strong fluorescence [32]. Triphenylamine has various properties such as high fluorescence quantum yields, visible region wavelength, strong UV-vis and luminescent properties, which are useful characteristics for developing chemosensors [33–39]. Chalcone structure is known for optically active structure [40–42]. Also, a conjugate π-electronic system of this structure provides the chelating ability for metal ions [43–45]. Due to these properties, the chalcone structure is useful to develop chemosensors detecting metal ions [45, 46]. Pd²⁺ is known as a fluorescent quencher [47–49]. This property is useful for the development of a sensor that detects Pd²⁺ through quenching [50]. Therefore, we expected that the combination of the pyridine and the chalcone structure having triphenylamine might produce a sensor that detects Pd²⁺ with turn-off.

Herein, we present a fluorescent and colorimetric chemosensor **DiPP** for detecting Pd²⁺. **DiPP** was the first chalcone-based chemosensor to detect Pd²⁺ through both fluorescence and color change methods. Chemosensor **DiPP** was able to detect Pd²⁺ with low detection limits (0.67 μM and 0.80 μM) by fluorescence turn-off and colorimetric variation of yellow to purple. Also, the test strip absorbed with **DiPP**

✉ Cheal Kim
  chealkim@snut.ac.kr

[1] Dept of New and Renewable Energy Convergence and Fine Chem, Seoul National Univ. of Sci. and Tech. (SNUT), 01811 Seoul, Korea
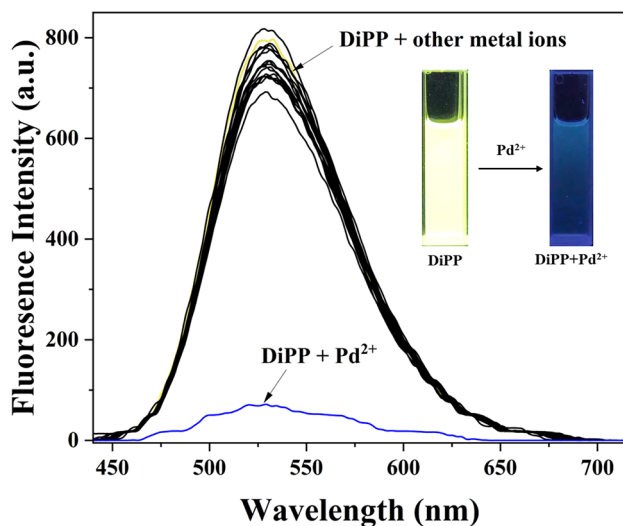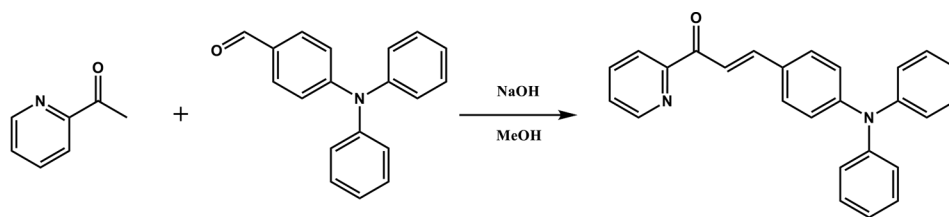
Scheme 1 Synthesis of DiPP

Fig. 1 Fluorescent intensity variations of DiPP (2.0 μM) with cations (15 equiv; λ_{ex} = 418 nm)

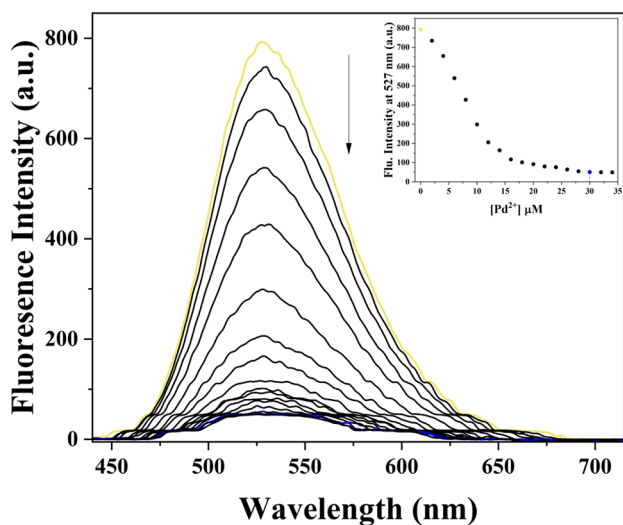

Fig. 2 Fluorescent variations of **DiPP** (2.0 μM) with varied amounts of Pd^{2+} (λ_{ex} = 418 nm)

could detect Pd^{2+} easily and quickly through fluorescence turn-off and color change. The binding feature of **DiPP** to
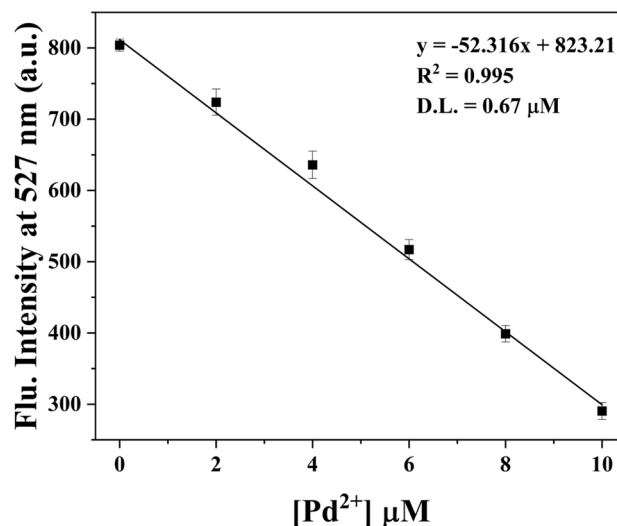

Fig. 3 Analysis of the detection limit for Pd^{2+} by **DiPP** (2 μM) based on the fluorescence intensity at 527 nm (λ_{ex} = 418 nm). The standard deviations are represented by the error bar (n = 3)

Pd^{2+} was addressed by UV-visible titrations, ESI-mass, ^{1}H NMR titration, DFT calculations and Job plot.

Experimental Section

General

Chemicals were commercially acquired from Alfa Aesar and TCI. ^{13}C and ^{1}H NMR spectra were gained with a Varian spectrometer. With Perkin Elmer spectrometers, emission and absorption data were recorded. A Thermo MAX instrument provided ESI-MS spectra.

Synthesis of Sensor DiPP ((*E*)-3-(4-(Diphenylamino) Phenyl)-1-(Pyridin-2-yl)prop-2-en-1-one)

DiPP was synthesized according to the literature method [51]. 2-Acetylpyridine (342 μL, 3.0 × 10^{-3} mol) and 5 mL of 10% NaOH were added in 15 mL of MeOH. The solution was stirred for 50 min. 4-(Diphenylamino)benzaldehyde (558 mg, 2.0 × 10-3 mol) was added to the solution. The mixture was stirred at 20 ºC for 16 h. An orange powder was washed with ether several times and dried in the oven. The
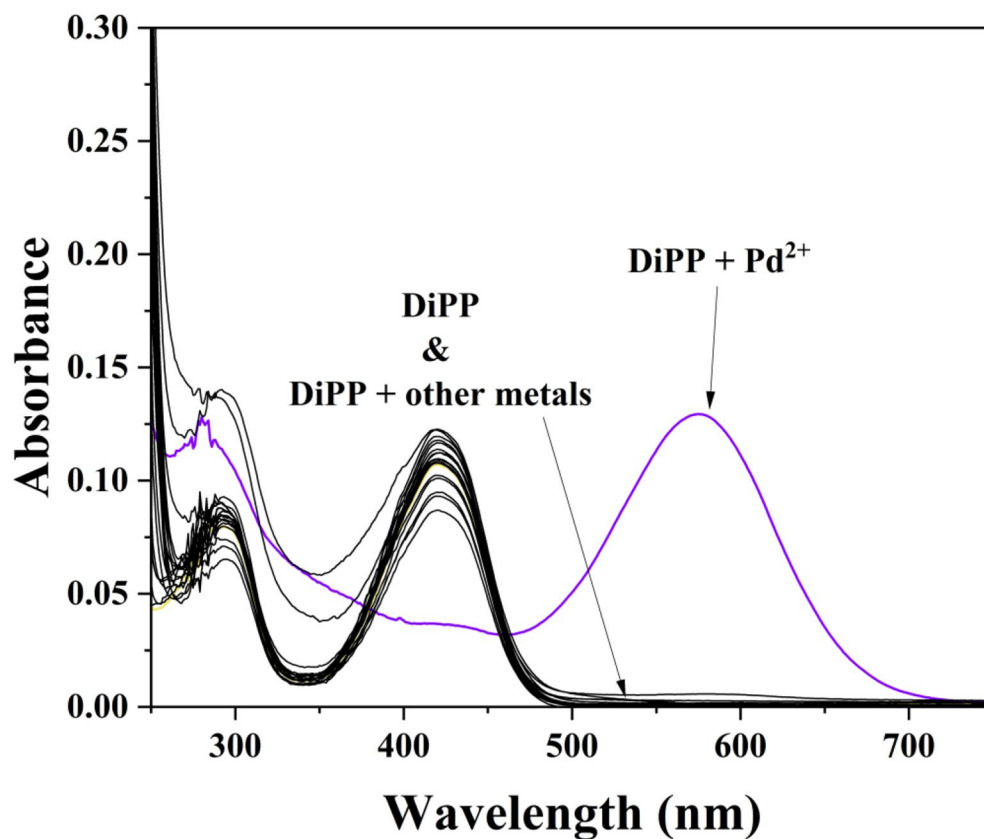
(a)

(b)

Fig. 4 (a) UV-vis absorbance variations of **DiPP** (5.0 μM) with varied cations (3.6 equiv). (b) Color changes of **DiPP** (5.0 μM) with cations (3.6 equiv)

dried powder was dissolved in chloroform and purified by column chromatography using chloroform. Yield: 436 mg (58%). ^{1}H NMR in CD_3CN: 8.79–8.77 (d, 1 H), 8.13–8.08 (m, 2 H), 8.06–8.02 (t, 1 H), 7.81–7.77 (d, 1 H), 7.71–7.66 (m, 3 H), 7.40–7.36 (m, 4 H), 7.18–7.11 (m, 6 H), 6.92–6.90 (d, 2 H). ^{13}C NMR in deuterated DMSO:188.5 (1 C), 153.8 (1 C), 150.0 (1 C), 149.2 (1 C), 146.3 (2 C), 144.1 (1 C), 137.8 (1 C), 130.5 (2 C), 130.0 (4 C), 127.6 (1 C),
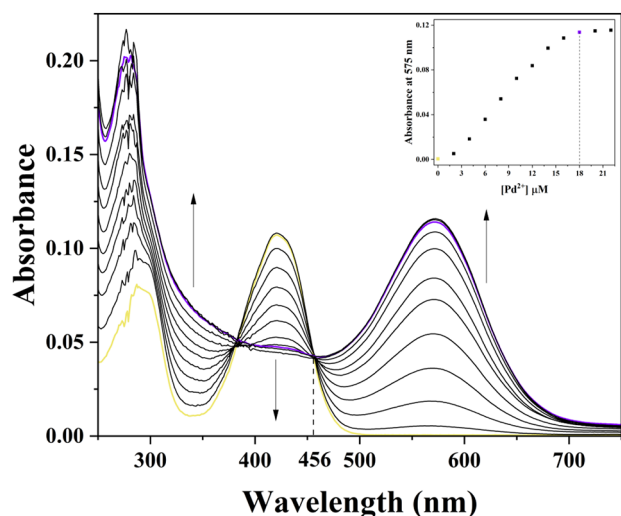
Fig. 5 UV-vis variations of **DiPP** (5.0 μM) with different concentrations of Pd^{2+}

127.4 (1 C), 125.6 (4 C), 124.7 (2 C), 122.5 (1 C), 120.6 (2 C). ESI-mass: calcd for $([DiPP+H^{+}+2H_{2}O+2THF])^{+}$: 557.30, found 557.58.

Fluorescent and UV-vis Titrations

6 μL (1 mM) of **DiPP** (3.8 mg, 1×10^{-5} mol) dissolved in 10 mL of tetrahydrofuran (THF) was diluted in 2.994 mL THF to provide 2×10^{-6} M. 3–54 μL (2×10^{-3} M) of $Pd(NO_3)_2$ (2.5 mg) dissolved in THF (5.0 mL) were added to **DiPP** (3 mL, 2×10^{-6} M). Their fluorescence spectra were taken in 10 s. For UV-vis, 15 μL (1 mM) of **DiPP** (1×10^{-5} mol, 3.8 mg) dissolved in 10 mL of THF was diluted in 2.985 mL THF to provide 5×10^{-6} M. 3–33 μL (0.4–4.4 eq) of $Pd(NO_3)_2$ (2 mM) dissolved in THF were added to **DiPP** (3 mL, 5×10^{-6} M). Their UV-visible spectra were taken in 10 s.

Competition

DiPP (1×10^{-5} mol, 3.8 mg) was dissolved in 10 mL of THF. 0.06 mmol of KNO_3, $NaNO_3$, $In(NO_3)_3$, $Cr(NO_3)_3$, $Ga(NO_3)_3$, $Fe(NO_3)_3$, $Al(NO_3)_3$, $Hg(NO_3)_2$, $Ni(NO_3)_2$, $Ca(NO_3)_2$, $Co(NO_3)_2$, $Mn(NO_3)_2$, $Cu(NO_3)_2$, $Cd(NO_3)_2$, $Pb(NO_3)_2$, $Mg(NO_3)_2$, $Zn(NO_3)_2$, and $Pd(NO_3)_2$ was dissolved in 3,000 μL THF. 4.5 μL of each metal (2×10^{-2} M) and Pd^{2+} ion (2×10^{-2} M) was added into 2,985 μL THF to afford 15 equiv. 6 μL (1×10^{-3} M) of the **DiPP** stock was added to the solutions. Their fluorescence spectra were taken in 10 s. For the UV-vis, 2.7 μL of each metal (2×10^{-2} M) and Pd^{2+} ion (2×10^{-2} M) was added into 2,980 μL THF to afford 3.6 equiv. 15 μL (1×10^{-3} M) of the **DiPP** stock was added to the solutions. Their UV-visible spectra were taken in 10 s.

Quantum Yields of DiPP and DiPP-Pd^{2+}

Standard fluorophore fluorescein ($\Phi_F = 0.79$) was used for quantum yield [47].

$$\Phi_{F(X)} = \Phi_{F(S)}(A_S F_X / A_X F_S)\,(n_X/n_S)^2$$

(Φ_F: fluorescence quantum yield, s: standard, A: absorbance, n: refractive index of the solvent, F: area of fluorescence emission curve and x: unknown)

Job Plot

A stock solution of sensor **DiPP** (1 mM) was prepared in 10 mL of THF. Pd^{2+} solution (1×10^{-3} M) with nitrate salt was acquired in 10 mL of THF. 3–27 μL of the **DiPP** stock was transferred to several quartzes. $27-3$ μL of the Pd^{2+} stock was added to diluted **DiPP**. THF was added to each quartz up to 3,000 μL. Fluorescence spectra of the solutions mixed were taken in 10 s.

^{1}H NMR Titration

Two NMR tube of **DiPP** (3.8 mg, 1×10^{-5} mol) dissolved in CD_3CN (250 μL) was prepared. In one tube, 250 μL of CD_3CN was added to make a 20 mM **DiPP** sample. In the other tube, $Pd(NO_3)_3$ (2.3 mg, 1×10^{-5} mol) dissolved in CD_3CN (250 μL) added to prepare a 20 mM **DiPP**-Pd^{2+} sample. ^{1}H NMR data were recorded in 10 s.

Calculations

To investigate the detecting mechanism of **DiPP** to Pd^{2+}, the Gaussian16 program [53] was used for calculations. They were based on m06 density functional [54–56]. 6-31G(d,p) [57, 58] and Lanl2DZ [59] basis sets were employed for calculations of Pd^{2+} and elements. The solvent effect on THF was considered by employing IEFPCM [60]. With the optimized features of **DiPP** and **DiPP**-Pd^{2+}, 20 of the lowest singlet-singlet transitions were calculated with TD-DFT to study the transition states of **DiPP** and **DiPP**-Pd^{2+}.

Results and Discussion

Molecule **DiPP** was gained through the aldol condensation of 4-(diphenylamino)benzaldehyde with 2-acetylpyridine (Scheme 1). **DiPP** was affirmed by ^{1}H NMR, ^{13}C NMR, and ESI-MS (Figs. S1-S3).

Fluorescent selectivity of **DiPP** was studied with diverse cations (K^+, Ag^+, Cu^{2+}, Co^{2+}, Zn^{2+}, Cd^{2+}, Ca^{2+}, Mn^{2+}, Mg^{2+}, Pb^{2+}, Ni^{2+}, Hg^{2+}, Cr^{3+}, Ga^{3+}, Na^+, In^{3+}, Fe^{3+}, Al^{3+}, and Pd^{2+}) in THF. As exhibited in Fig. 1, **DiPP** and **DiPP** with most metals represented strong fluorescence at 527 nm ($\lambda_{ex} = 418$ nm). By contrast, Pd^{2+} showed a clear quenching
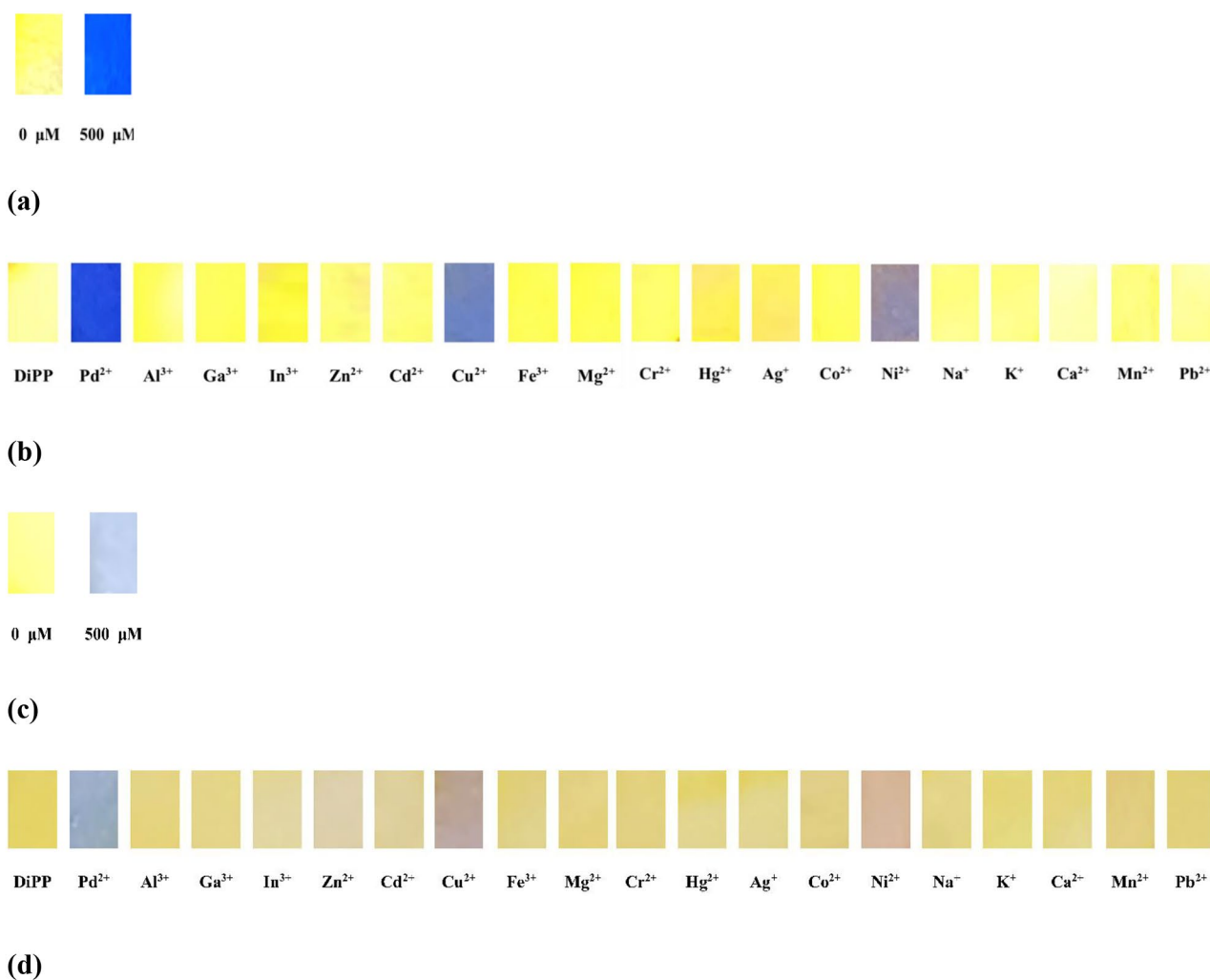
Fig. 6 Photographs of **DiPP**-coated test strips (1 mM). (a) **DiPP**-test strips immersed in Pd²⁺ (0 and 500 µM) under UV light. (b) **DiPP**-test strips were immersed in varied metal ions (500 µM) under UV light. (c) Color variation of DiPP-test strips immersed in Pd²⁺ (0 and 500 µM). (d) Color change of DiPP-test strips immersed in varied metal ions (500 µM)

with **DiPP** at 527 nm. The quantum yields (Φ) of **DiPP** and **DiPP**-Pd²⁺ were given to be 0.71 and 0.088, respectively. Thus, **DiPP** worked as a fluorescent turn-off chemosensor for the obvious probing of Pd²⁺. To study the photophysical feature of **DiPP** to Pd²⁺, fluorescent titrations were checked (Fig. 2). The fluorescence of **DiPP** at 527 nm smoothly decreased until Pd²⁺ increased to 15 equiv (Fig. 2). The decrease in fluorescence intensity of **DiPP** with the increasing amount of Pd²⁺ ions was proposed as chelation enhanced quenching (CHEQ) mechanism. The developed sensor determined Pd²⁺ in the linear range of 0–10 µM, with a low detection limit of 0.67 µM (3_σ/k) (R² = 0.995) (Fig. 3) [61]. A competitive test was performed to know if **DiPP** could exclusively bind to Pd²⁺ with the other coexisting metals (Fig. S4). Most cations did not display the binding of

DiPP to Pd²⁺. However, about 50% of the interference was observed from Cr³⁺ and more than 90% from K⁺ ions.

To check the colorimetric probing of **DiPP** to Pd²⁺, the UV-vis variation was studied with diverse cations in THF (Fig. 4). **DiPP** and **DiPP** with most cations showed no or little absorbance at 575 nm. However, the addition of Pd²⁺ caused an obvious increase in absorbance at 575 nm and a colorimetry variation of pale yellow to purple. Therefore, **DiPP** could also be performed as a colorimetry chemosensor for the nicely selective probing of Pd²⁺. Importantly, as far as we know, **DiPP** is the first chalcone structure-based probe among chemosensors to detect Pd²⁺ through both fluorescence and color change methods. (Table S1).

To understand the colorimetric sensing feature of **DiPP** to Pd²⁺, UV-vis titrations were tested (Fig. 5). Absorbance of **DiPP** at 340 and 575 nm obviously increased, and that of
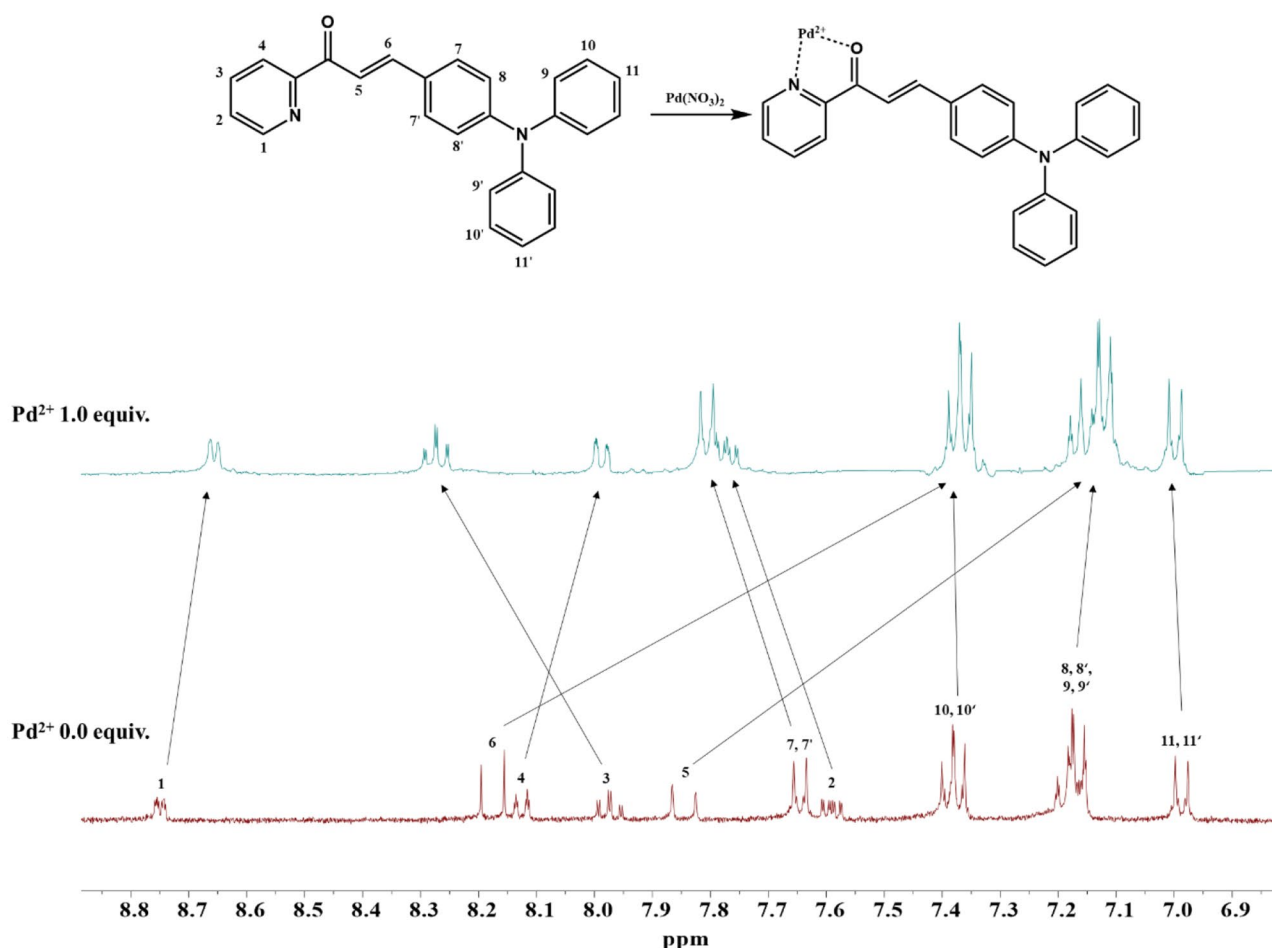
Fig. 7 ^{1}H NMR titration of **DiPP** with Pd^{2+} (0 and 1.0 equiv)

425 nm decreased until the amount of Pd^{2+} got to 3.6 equiv. A sound isosbestic point at 456 nm signified that the combination of **DiPP** with Pd^{2+} formed a species. The detection limit of **DiPP** with Pd^{2+} based absorbance change was calculated to be 0.80 μM (3$_σ$/k) in the range from 0 to 14 μM (R^2 = 0.995) (Fig. S5) [61].

A competitive test was achieved to know whether **DiPP** could exclusively bind to Pd^{2+} among the coexisting metals for colorimetric chemosensors (Fig. S6). The color change was not disturbed by most metals but was disturbed by 50% from Cr^{3+} and 75% from K$^+$ ions. For the practical test, filter papers coated with **DiPP** were employed. The test strips could probe Pd^{2+} via a fluorescence turn-off and a colorimetry change from yellow to light navy blue (Fig. 6). Cu^{2+} and Ni^{2+} showed some inhibition in the fluorescent test kit. Thus, the **DiPP**-coated test strip can have the practical application to rapidly and readily recognize Pd^{2+}.

Detecting Mechanism of DiPP to Pd^{2+}

To determine the reaction ratio of **DiPP** with Pd^{2+}, a Job plot method was applied and showed the biggest value at a 0.5 molar fraction (Fig. S7). It meant that a Pd^{2+} bound to a **DiPP** with a 1 : 1 ratio. Positive-ion ESI-MS displayed that the peaks of 626.18 (m/z) and 756.49 (m/z) corresponded to [**DiPP** + Pd^{2+} + NO$_3^-$ + 2MeOH + H$_2$O]$^+$ (calcd, 626.11) and [**DiPP** + Pd^{2+} + NO$_3^-$ + MeOH + 2H$_2$O + 2THF]$^+$ (calcd, 756.21) (Fig. S8). In addition, the ^{1}H NMR titration was applied to illustrate how to interact **DiPP** with Pd^{2+} (Fig. 7). As the Pd^{2+} were added, the protons H$_1$ and H$_4$ showed an up-field shift, whereas H$_2$ and H$_3$ moved down-field. The protons H$_5$ and H$_6$ showed a large up-field shift, respectively. In contrast, the protons of tri-phenyl amine showed relatively small movement to the down-field, except for H$_7$ and H$_{7'}$, which were close to the binding site. The outcomes drove us to suppose that Pd^{2+} may bind with the nitrogen of the pyridine moiety and the oxygen of the carbonyl group. The binding constants of the **DiPP**-Pd^{2+}

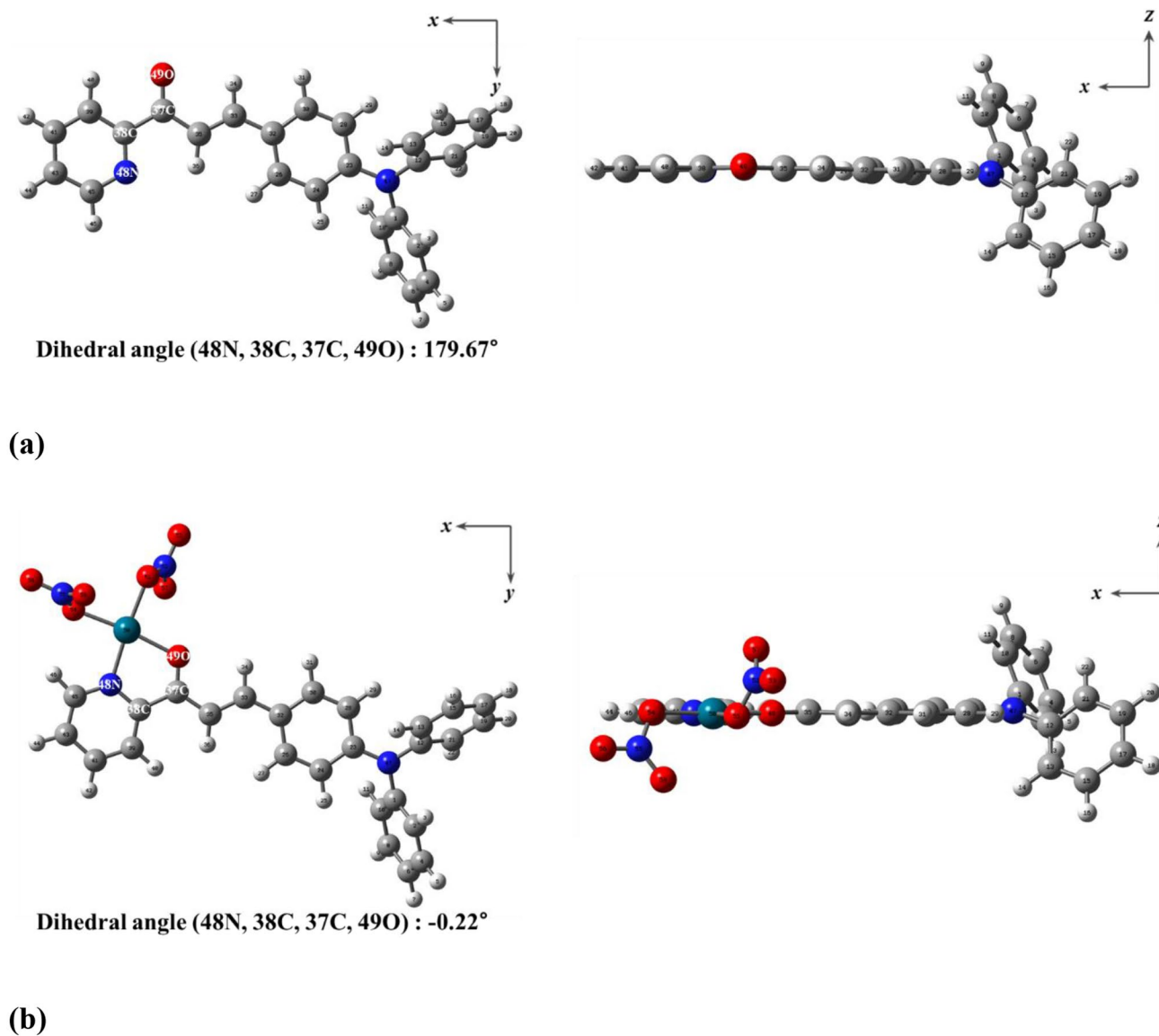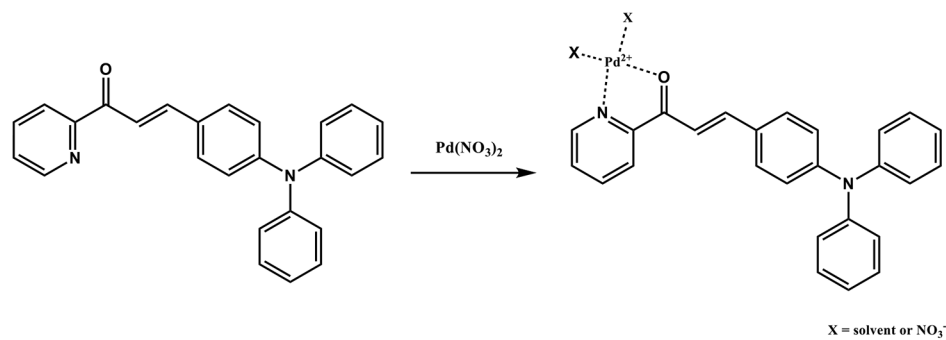Dihedral angle (48N, 38C, 37C, 49O) : 179.67°

(a)

Dihedral angle (48N, 38C, 37C, 49O) : -0.22°

(b)

Fig. 8 Energy-optimized forms of (a) DiPP and (b) DiPP-Pd^{2+}

Scheme 2 Proposed structure of DiPP-Pd^{2+}

X = solvent or NO$_3^-$

complex were given to be 7.0×10^4 M^{-1} based on fluorescence intensity and 1.7×10^4 M^{-1} based on UV-vis absorbance from the Benesi-Hildebrand equation (Figs. S9 and S10). With Job plot, ESI-MS, and ^{1}H NMR titration, the likely feature of **DiPP**-Pd^{2+} was supposed (Scheme 2).

Calculations

To demonstrate the sensing feature of **DiPP** to Pd^{2+}, theoretical calculations of **DiPP** and **DiPP**-Pd^{2+} were achieved. The 1:1 association of **DiPP** and Pd^{2+} was applied to calculations of **DiPP**-Pd^{2+}, which was supposed by Job plot and ESI-MS. The optimized features of **DiPP** and **DiPP**-Pd^{2+} are demonstrated in Fig. 8. The dihedral angle (48 N, 38 C, 37 C, and 49O) of **DiPP** is calculated as 179.67 °, indicating that the carbonyl oxygen and the pyridine nitrogen are in the plane. In the **DiPP**-Pd^{2+} complex, **DiPP** as a bidentate ligand chelates Pd^{2+} using the pyridine nitrogen and the carbonyl oxygen, and two NO$_3^-$ are bound in the vacant sites. As a result, the optimized **DiPP**-Pd^{2+} complex showed a square planar structure. With the optimized features, TD-DFT calculations were carried out for studying the electron transitions of **DiPP** and **DiPP**-Pd^{2+}. For **DiPP**, the HOMO → LUMO transition of 441.47 nm was regarded as the major transition, showing an ICT character (Figs. S11 and S12). Its molecular orbitals (MOs) displayed the shift of the electron cloud from the triphenylamine moiety to the pyridine one. This ICT character leads to the yellow color of **DiPP**. For **DiPP**-Pd^{2+}, the HOMO → LUMO related to the 558.94 nm showed a similar ICT property to free **DiPP** (Figs. S12 and S13). The energy gap between HOMO and LUMO was decreased when the **DiPP**-Pd^{2+} complex was formed (Fig. S12). Therefore, the color variation of yellow to purple in **DiPP**-Pd^{2+} might be due to the change of bandgap energy, resulting in a redshift. With ESI-MS, Job plot, calculations, and ^{1}H NMR titration, we proposed the binding feature of Pd^{2+} to **DiPP** (Scheme 2).

Conclusion

We addressed a chemosensor **DiPP** based on a chalcone structure having triphenylamine that can exclusively detect Pd^{2+} by a fluorescent turn-off and colorimetry variation of pale yellow to purple. The association ratio of **DiPP** to Pd^{2+} was analyzed to be a 1: 1 ratio with ESI-MS and Job plot. The calculated detection limits of **DiPP** for Pd^{2+} were 0.67 μM and 0.80 μM through fluorescence and colorimetry. Specifically, it is noteworthy that **DiPP** could exclusively distinguish Pd^{2+} from in the same group Ni^{2+}. Also, the colorimetric and fluorescent test strips coated with **DiPP** rapidly and easily recognized Pd^{2+}. Interestingly, **DiPP** was the

first chalcone-based fluorescent and colorimetric probe to detect Pd^{2+}. The binding mechanisms of **DiPP** to Pd^{2+} could be supposed through NMR titration, Job plot, DFT calculations, fluorescent and UV-visible titrations, and ESI-mass.

Declarations

Ethics approval and consent to participate Not applicable.

Consent for publication Not applicable.

Competing interests The authors declare no competing interests.

References

1. Wang M, Liu X, Lu H et al (2015) Highly selective and reversible chemosensor for Pd^{2+} detected by fluorescence, colorimetry, and test paper. ACS Appl Mater Interfaces 7:1284–1289. https://doi.org/10.1021/am507479m

2. Zhou Y, Zhang J, Zhou H et al (2012) A highly sensitive and selective "off-on" chemosensor for the visual detection of Pd^{2+} in aqueous media. Sens Actuators B Chem 171–172:508–514. https://doi.org/10.1016/j.snb.2012.05.021

3. Kim H, Moon KS, Shim S, Tae J (2011) Cyclen-conjugated rhodamine hydroxamate as Pd^{2+}-specific fluorescent chemosensor. Chem - An Asian J 6:1987–1991. https://doi.org/10.1002/asia.201100126

4. Tang FK, Chan SM, Wang T et al (2020) Highly selective detection of Pd^{2+} ion in aqueous solutions with rhodamine-based colorimetric and fluorescent chemosensors. Talanta 210:120634. https://doi.org/10.1016/j.talanta.2019.120634

5. Kumar A, Virender, Mohan B et al (2022) Development of 2-hydroxy-naphthaldehyde functionalized Schiff base chemosensor for spectroscopic and colorimetric detection of Cu^{2+} and Pd^{2+} ions. Microchem J 180:107561. https://doi.org/10.1016/j.microc.2022.107561

6. Popov LD, Karlutova OY, Shepelenko EN et al (2020) Selective Naked-Eye Fluorescein-Based Chemosensor for the detection of Pd^{2+} cations. Dokl Chem 490:23–26. https://doi.org/10.1134/S0012500820020032

7. Chen H, Jin X, Zhang W et al (2018) A new rhodamine B-based 'off-on' colorimetric chemosensor for Pd^{2+} and its imaging in living cells. Inorg Chim Acta 482:122–129. https://doi.org/10.1016/j.ica.2018.05.032

8. Liu K, Hu Z (2020) A Novel Conjugated Polymer Consists of Benzimidazole and Benzothiadiazole: synthesis, Photophysics

Properties, and Sensing Properties for Pd²⁺. J Polym Sci Part A Polym Chem 831–842. https://doi.org/10.1002/pol.20200005

9. Wang L, Zheng XY, Zhang X, Zhu ZJ (2021) A quinoline-based fluorescent chemosensor for palladium ion (Pd²⁺)-selective detection in aqueous solution. Spectrochim Acta A Mol Biomol Spectrosc 249:119283. https://doi.org/10.1016/j.saa.2020.119283

10. Wu S, Jiang H, Zhang Y et al (2021) A novel "on-off-on" acylhydrazone-based fluorescent chemosensor for ultrasensitive detection of Pd²⁺. J Mol Liq 327:114836. https://doi.org/10.1016/j.molliq.2020.114836

11. Li P, Li R, Wang K et al (2022) A julolidine-chalcone-based fluorescent probe for detection of Al³⁺ in real water sample and cell imaging. Spectrochim Acta A Mol Biomol Spectrosc 276:121213. https://doi.org/10.1016/j.saa.2022.121213

12. Pungut NAS, Heng MP, Saad HM et al (2021) From one to three, modifications of sensing behavior with solvent system: DFT calculations and real-life application in detection of multianalytes (Cu²⁺, Ni²⁺ and Co²⁺) based on a colorimetric Schiff base probe. J Mol Struct 1238:130453. https://doi.org/10.1016/j.molstruc.2021.130453

13. Adak AK, Dutta B, Manna SK, Sinha C (2019) Rhodamine-appended Benzophenone Probe for Trace Quantity detection of Pd²⁺ in living cells. ACS Omega 4:18987–18995. https://doi.org/10.1021/acsomega.9b01860

14. Wu H, Lin L, Zheng L et al (2022) Dual-response fluorescence sensor for detecting Cu²⁺ and Pd²⁺ based on bis-tetraphenylimidazole Schiff-base. J Photochem Photobiol A Chem 432:114076. https://doi.org/10.1016/j.jphotochem.2022.114076

15. B S K SS, Makam P et al (2021) Highly sensitive and Rapid detection of mercury in water using functionalized etched fiber Bragg grating sensors. Sens Actuators B Chem 333:129550. https://doi.org/10.1016/J.SNB.2021.129550

16. He L, Tao H, Koo S et al (2018) Multifunctional fluorescent nanoprobe for sequential detections of Hg²⁺ ions and biothiols in live cells. ACS Appl Bio Mater 1:871–878. https://doi.org/10.1021/acsabm.8b00300

17. Guan WL, Zhang YF, Zhang QP et al (2022) A novel fluorescent chemosensor based on naphthofuran functionalized naphthalimide for highly selective and sensitive detecting Hg²⁺ and CN⁻. J Lumin 244:118722. https://doi.org/10.1016/j.jlumin.2021.118722

18. Jung JM, Kim C, Harrison RG (2018) A dual sensor selective for Hg²⁺ and cysteine detection. Sens Actuators B Chem 255:2756–2763. https://doi.org/10.1016/J.SNB.2017.09.090

19. Kang JH, Kim C (2018) Colorimetric detection of iron and fluorescence detection of zinc and cadmium by a chemosensor containing a bio-friendly octopamine. Photochem Photobiol Sci 17:442–452. https://doi.org/10.1039/C7PP00468K

20. Zhang L, Wang C, Jiang Y et al (2022) Selective and sensitive detection and detoxification of Pd²⁺ in living cells with a water-soluble fluorescent probe. Anal Chim Acta 1204:339728. https://doi.org/10.1016/j.aca.2022.339728

21. Kang JH, Han J, Lee H et al (2018) A water-soluble fluorescence chemosensor for the sequential detection of Zn²⁺ and pyrophosphate in living cells and zebrafish. Dyes Pigm 152:131–138. https://doi.org/10.1016/J.DYEPIG.2018.01.039

22. Chae JB, Yun D, Kim S et al (2019) Fluorescent determination of zinc by a quinoline-based chemosensor in aqueous media and zebrafish. Spectrochim Acta A Mol Biomol Spectrosc 219:74–82. https://doi.org/10.1016/J.SAA.2019.04.044

23. Li L, Guan R, Guo M et al (2018) A FRET based two-photon fluorescent probe for ratiometric detection of Pd²⁺ in living cells and in vivo. Sens Actuators B Chem 254:949–955. https://doi.org/10.1016/j.snb.2017.07.157

24. Mondal S, Manna SK, Pathak S et al (2019) A colorimetric and "off-on" fluorescent Pd²⁺ chemosensor based on a rhodamine-ampyrone conjugate: synthesis, experimental and theoretical studies along with in vitro applications. New J Chem 43:3513–3519. https://doi.org/10.1039/c8nj05194a

25. Chen Y, Chen B, Han Y (2016) A novel rhodamine-based fluorescent probe for the fluorogenic and chromogenic detection of Pd²⁺ ions and its application in live-cell imaging. Sens Actuators B Chem 237:1–7. https://doi.org/10.1016/j.snb.2016.06.067

26. Kim BY, Pandith A, Cho CS, Kim HS (2019) Highly selective fluorescent probe based on 2-(2′-Dansylamidophenyl)-Thiazole for sequential sensing of copper(II) and iodide ions. Bull Korean Chem Soc 40:163–168. https://doi.org/10.1002/BKCS.11663

27. Ko YG, Mayank, Singh N, Jang DO (2018) Single chemosensor for sensing multiple analytes: selective fluorogenic detection of Cu²⁺ and Br⁻. Tetrahedron Lett 59:3839–3844. https://doi.org/10.1016/j.tetlet.2018.09.024

28. Finelli A, Chabert V, Hérault N et al (2019) Sequential multiple-target sensor: In³⁺, Fe²⁺, and Fe³⁺ discrimination by an anthracene-based probe. Inorg Chem 58:13796–13806. https://doi.org/10.1021/ACS.INORGCHEM.9B01478/ASSET/IMAGES/LARGE/IC9B01478_0008.JPEG

29. Kumar R, Jain H, Gahlyan P et al (2018) A highly sensitive pyridine-dicarbohydrazide based chemosensor for colorimetric recognition of Cu²⁺, AMP²⁻, F⁻ and AcO⁻ ions. New J Chem 42:8567–8576. https://doi.org/10.1039/c8nj00918j

30. Kim H, Suh B, Kim C (2022) A pyridine-dicarbohydrazide-based chemosensor for detecting Al³⁺ by fluorescence turn-on. J Chin Chem Soc 69:366–374. https://doi.org/10.1002/JCCS.202100374

31. Kim A, Kang JH, Jang HJ, Kim C (2018) Fluorescent detection of zn(II) and in(III) and colorimetric detection of Cu(II) and Co(II) by a versatile chemosensor. J Ind Eng Chem 65:290–299. https://doi.org/10.1016/j.jiec.2018.04.040

32. Duraimurugan K, Harikrishnan M, Madhavan J et al (2021) Anthracene-based fluorescent probe: synthesis, characterization, aggregation-induced emission, mechanochromism, and sensing of nitroaromatics in aqueous media. Environ Res 194:110741. https://doi.org/10.1016/j.envres.2021.110741

33. Xia Y, Zhang H, Zhu X et al (2018) A highly selective two-photon fluorescent chemosensor for tracking homocysteine via situ reaction. Dyes Pigm 155:159–163. https://doi.org/10.1016/j.dyepig.2018.03.034

34. Mishra A, Dheepika R, Parvathy PA et al (2021) Fluorescence quenching based detection of nitroaromatics using luminescent triphenylamine carboxylic acids. Sci Rep 11:1–10. https://doi.org/10.1038/s41598-021-97832-0

35. Chen H, Yang P, Li Y et al (2020) Insight into triphenylamine and coumarin serving as copper (II) sensors with "OFF" strategy and for bio-imaging in living cells. Spectrochim Acta A Mol Biomol Spectrosc 224:117384. https://doi.org/10.1016/j.saa.2019.117384

36. Santiwat T, Sornkaew N, Mayurachayakul P et al (2022) A new triphenylamine-pyrenyl salicylic acid fluorophore for the detection of highly selective Cu(II) ions in an aqueous media at the picomolar level. J Mol Struct 1259:132735. https://doi.org/10.1016/j.molstruc.2022.132735

37. Liu B, Tan Y, Hu Q et al (2019) A naked eye fluorescent chemosensor for Zn²⁺ based on triphenylamine derivative and its bioimaging in live cells. Chem Pap 73:3123–3134. https://doi.org/10.1007/s11696-019-00853-3

38. Jiang Y, Zhang S, Wang B et al (2018) Novel triphenylamine-based fluorescent probe for specific detection and bioimaging of OCl⁻. Tetrahedron 74:5733–5738. https://doi.org/10.1016/j.tet.2018.08.010

39. Mathivanan M, Tharmalingam B, Mani KS et al (2020) Simple C₃-symmetric triaminoguanidine-triphenylamine conjugate as an efficient colorimetric sensor for Cu(II) and fluorescent sensor for Fe(III) ions. Spectrochim Acta A Mol Biomol Spectrosc 234:118235. https://doi.org/10.1016/j.saa.2020.118235

40. Gupta A, Garg S, Singh H et al (2020) Development of chalcone-based derivatives for sensing applications. Anal Methods 12:5022–5045. https://doi.org/10.1039/d0ay01603a

41. Chen H, Fang S, Wang L et al (2021) Tetraphenylene-chalcone hybrid derivatives: synthesis, structural, fluorescence properties and imaging in living cells. J Mol Liq 321:114913. https://doi.org/10.1016/j.molliq.2020.114913

42. El-Nahass MN (2021) D–π–A chalcone analogue metal ions selective turn-on-off-on fluorescent chemosensor with cellular imaging and corrosion protection. J Mol Struct 1239:130527. https://doi.org/10.1016/j.molstruc.2021.130527

43. Sulpizio C, Breibeck J, Rompel A (2018) Recent progress in synthesis and characterization of metal chalcone complexes and their potential as bioactive agents. Coord Chem Rev 374:497–524. https://doi.org/10.1016/j.ccr.2018.05.023

44. Singh G, Singh J, Mangat SS et al (2015) Chalcomer assembly of optical chemosensors for selective Cu^{2+} and Ni^{2+} ion recognition. RSC Adv 5:12644–12654. https://doi.org/10.1039/c4ra14329a

45. Singh G, Arora A, Rani S et al (2017) A click-generated Triethoxysilane Tethered Ferrocene-Chalcone-Triazole Triad for selective and colorimetric detection of Cu^{2+} ions. ChemistrySelect 2:3637–3647. https://doi.org/10.1002/slct.201700186

46. Asiri AM, Al-amari MM, Ullah Q, Salman A (2020) Ultrasound-assisted synthesis and photophysical investigation of a heterocyclic alkylated chalcone: a sensitive and selective fluorescent chemosensor for Fe^{3+} in aqueous media. J Coord Chem 73:2987–3002. https://doi.org/10.1080/00958972.2020.1838490

47. Mahapatra AK, Manna SK, Maiti K et al (2015) An azodye-rhodamine-based fluorescent and colorimetric probe specific for the detection of Pd^{2+} in aqueous ethanolic solution: synthesis, XRD characterization, computational studies and imaging in live cells. Analyst 140:1229–1236. https://doi.org/10.1039/c4an01575d

48. Goswami S, Sen D, Das NK et al (2011) A new rhodamine based colorimetric "off-on" fluorescence sensor selective for Pd^{2+} along with the first bound X-ray crystal structure. Chem Commun 47:9101–9103. https://doi.org/10.1039/c1cc12845k

49. Yang M, Bai Y, Meng W et al (2014) A novel selective fluorescent and colorimetric chemosensor for the visual detection of Pd^{2+} and application of imaging in living cells. Inorg Chem Commun 46:310–314. https://doi.org/10.1016/j.inoche.2014.06.027

50. Mahata S, Bhattacharya A, Kumar JP et al (2020) Naked-eye detection of Pd^{2+} ion using a highly selective fluorescent heterocyclic probe by "turn-off" response and in-vitro live cell imaging. J Photochem Photobiol A Chem 394:112441. https://doi.org/10.1016/j.jphotochem.2020.112441

51. Liang ZQ, Wang XM, Dai GL et al (2015) The solvatochromism and aggregation-induced enhanced emission based on triphenylamine-propenone. New J Chem 39:8874–8880. https://doi.org/10.1039/c5nj01072a

52. Magde D, Wong R, Seybold PG (2002) Fluorescence Quantum Yields and Their Relation to Lifetimes of Rhodamine 6G and Fluorescein in Nine Solvents: Improved Absolute Standards for Quantum Yields¶. Photochem Photobiol 75:327. https://doi.org/10.1562/0031-8655(2002)075<0327:fqyatr>2.0.co;2

53. Frisch MJ, Trucks GW, Chlegel HB, Scuseria GE, Robb MA, Cheeseman JR, Scalmani G, Barone V, Petersson GA, Nakatsuji H, Li X, Caricato M, Marenich AV, Bloino J, Janesko BG, Gomperts R, Mennucci B, Hratchian HP, Ortiz, Izmay DJ (2016) Gaussian, Inc.

54. Kediya S, Manhas A, Jha PC (2022) Benzothiazole-based chemosensor: a quick dip into its anion sensing mechanism. J Phys Org Chem 35:27–29. https://doi.org/10.1002/poc.4283

55. Basri R, Ahmed N, Khalid M et al (2022) Quinoline based thiosemicarbazones as colorimetric chemosensors for fluoride and cyanide ions and DFT studies. Sci Rep 12:1–19. https://doi.org/10.1038/s41598-022-08860-3

56. Zhao Y, Truhlar DG (2008) The M06 suite of density functionals for main group thermochemistry, thermochemical kinetics, non-covalent interactions, excited states, and transition elements: two new functionals and systematic testing of four M06-class functionals and 12 other function. Theor Chem Acc 120:215–241. https://doi.org/10.1007/s00214-007-0310-x

57. Hariharan PC, Pople JA (1973) The influence of polarization functions on molecular orbital hydrogenation energies. Theor Chim Acta 28:213–222. https://doi.org/10.1007/BF00533485

58. Francl MM, Pietro WJ, Hehre WJ et al (1982) Self-consistent molecular orbital methods. XXIII. A polarization-type basis set for second-row elements. J Chem Phys 77:3654–3665. https://doi.org/10.1063/1.444267

59. Wadt WR, Hay PJ (1985) Ab initio effective core potentials for molecular calculations. Potentials for main group elements na to Bi. J Chem Phys 82:284–298. https://doi.org/10.1063/1.448800

60. Klamt A, Moya C, Palomar J (2015) A Comprehensive comparison of the IEFPCM and SS(V)PE Continuum Solvation Methods with the COSMO Approach. J Chem Theory Comput 11:4220–4225. https://doi.org/10.1021/acs.jctc.5b00601

61. Kim A, Kim C (2019) A hydrazono-quinoline-based chemosensor sensing In^{3+} and Zn^{2+} : Via fluorescence turn-on and ClO- via color change in aqueous solution. New J Chem 43:7320–7328. https://doi.org/10.1039/c9nj00899c